

# Egomotion Analysis Based on the Frenet–Serret Motion Model

Zoran Durić

Azriel Rosenfeld

Larry S. Davis

Computer Vision Laboratory  
Center for Automation Research  
University of Maryland  
College Park, MD 20742-3275

## Abstract

In this paper we propose a new model, *Frenet-Serret* motion, for the motion of an observer in a stationary environment. This model relates the motion parameters of the observer to the curvature and torsion of the path along which the observer moves. Screw-motion equations for Frenet-Serret motion are derived and employed for geometrical analysis of the motion. Normal flow is used to derive constraints on the rotational and translational velocity of the observer and to compute egomotion by intersecting these constraints in the manner proposed in [6]. The accuracy of egomotion estimation is analyzed for different combinations of observer motion and feature distance. We explain the advantages of controlling feature distance to analyze egomotion and derive the constraints on depth which make either rotation or translation dominant in the perceived normal flow field. The results of experiments on real image sequences are presented.

## 1 Introduction

The problem of egomotion estimation has been studied extensively in the past ten years [4, 7, 11, 14, 15, 16]. It is generally posed as follows: Given a sequence of images taken by a monocular observer undergoing continuous rigid motion in a stationary environment, recover the translation and rotation parameters of the observer (egomotion). Solutions to the egomotion estimation problem are based on both a model of the observer’s motion and the type of change in the sequence of images to be used for egomotion estimation.

The most general model of observer motion is unrestricted rigid motion, which can be represented by six parameters. In this case both rotation and translation are present [3]. If the motion of the observer is restricted in any way the number of parameters needed to represent it may be reduced, or coupling between the parameters may be introduced. The most common simplifications are that the motion is either *pure rotation* or *pure translation*. In both cases the number of parameters reduces to three. The methods employed to solve for egomotion in the case of pure rotation or pure translation would be more generally useful if there existed a reliable method of decoupling the rotational and translational parts of a general motion, since it is almost never the case, in naturally occurring motion, that the translation or rotation is exactly zero; however, no such method exists. If it could be determined when the translational (rotational) part of motion is “small” the methods for “pure” translational (rotational) motion could be used. However, a measure of smallness is not readily available. Another simplification is *planar motion*, in which the observer translates parallel to a plane and rotates about an axis normal to the plane. Here too, the motion is described by three parameters: one for rotation and two for translation. It was used in [5] to describe car motion.

We introduce a model called *Frenet-Serret motion* which corresponds to the motion of a moving trihedron (see Section 2) along a space curve. As long as the motion of the observer relative to the moving trihedron (e.g. rotation to change the observer’s viewing direction) is zero or known, the parameters of the motion are given by the curvature and torsion of the space curve along which the observer moves. Many special cases of Frenet-Serret motion

commonly occur. For example, when a land vehicle moves along a planar road its path is torsionless, and when it turns with banking its path has both curvature and torsion. An airborne vehicle moves along a space curve which may have both torsion and curvature. When it turns around its long axis, torsion is dominant; when it turns with banking, both torsion and curvature exist and are coupled by physical constraints. Since the parameters of the observer’s path depend on its speed, mass, size, and on the medium through which it moves, specific cases can be analyzed and bounds on curvature and torsion calculated. Additionally, it becomes possible to explicitly relate the relative dominance of rotation or translation to the parameters of the path and the distances to the features which are observed. We will show that  $R\lambda$ , where  $R$  is the distance of an observed feature from the observer and  $\lambda$  is the total curvature of the path, is a measure that can be used in practice to determine whether rotation or translation is, in fact, “small”.

Image velocities [2, 4, 7, 11, 12] and feature correspondences [14, 16] are commonly utilized for egomotion computation. Ideally the apparent motion, or image velocity field (what the observer can see), is the projection of the environmental motion field. Under this assumption, one tries to recover image velocities from sequences of images (either explicitly or implicitly) and to compute the required egomotion from the image velocity field. Direct methods (implicit velocity) are based on image derivatives [2, 7, 12] in conjunction with the motion constraint equation (*MCE*) [8]. Methods based on optic flow (explicit velocity) [4, 11] recover full velocity information and then compute egomotion. The steps which are followed in optic flow computation are: (i) spatial and temporal image derivatives are computed; (ii) using the *MCE*, the normal flow (the projection of the optic flow on the gradient direction) is computed; (iii) the optic flow is computed under the assumption that it is smooth, minimizing a cost function [8]. It is well known [8, 17] that the computed optic flow is in general different from the actual motion field. One can also see that even if the optic flow is smooth, there will usually exist many optic flow fields that are consistent with a given normal flow field; it is hard to determine which one is correct. To avoid errors in egomotion computation made by introducing an arbitrary cost function, we use normal flow directly. Based on a spherical projection model, we derive constraints on egomotion that allow us to solve the egomotion estimation problem by constraint intersection.

## 2 Model of the Motion

Here, we follow the derivation in [3]. If the environment is stationary and the observer is moving, the instantaneous velocity  $\dot{\vec{r}}_e$  of point  $\vec{r}_e$  in the environment relative to the observer is given by

$$\dot{\vec{r}}_e = -\vec{\Omega} \times \vec{r}_e - \vec{t} \quad (1)$$

where  $\vec{\Omega}$  is the instantaneous rotational velocity and  $\vec{t}$  is the instantaneous translational velocity. If the coordinate system is chosen in a different manner, then the equation of motion will change. The locus of the points

$$\vec{r}_c = \|\vec{\Omega}\|^{-2}(\vec{\Omega} \times \vec{t}) + \mu\vec{\Omega}$$

(where  $\mu$  is an arbitrary scalar) is called the *screw axis*. If the coordinate center is placed on this axis, then the translation is parallel to it and the equation of motion becomes

$$\dot{\vec{r}}_e = -\vec{\Omega} \times (\vec{r}_e - \vec{r}_c) - \sigma\vec{\Omega}.$$

The scalar

$$\sigma = \|\vec{\Omega}\|^{-2}(\vec{\Omega} \cdot \vec{t})$$

is called the *pitch* of the screw motion. The screw axis and the pitch of the screw motion are geometrical invariants of the first order for instantaneous motion.

The nodal point  $O$  of the observer moving through the environment is traveling along some space curve  $\gamma$ . If  $\gamma$  is smooth and twice differentiable, there is a natural coordinate system associated with this motion, defined by the tangent  $\vec{T}$ , normal  $\vec{N}$ , and binormal  $\vec{B}$  of the curve  $\gamma$  (see Figure 1a). The coordinate planes are: (i) the osculating plane defined by the tangent and normal, (ii) the normal plane defined by the normal and binormal, and (iii) the rectifying plane defined by the tangent and binormal. The natural coordinates  $(x(s), y(s), z(s))$ , where  $s$  is the arc length, determine  $\gamma$ . The triple  $(\vec{T}, \vec{N}, \vec{B})$  is called the moving trihedron. The point  $(x, y, z)$  can, through a suitable transformation, be written as  $(t, n, b)$  in the natural frame. The rotational motion of the moving trihedron is given by the

Frenet-Serret equations [10]

$$\begin{aligned}\dot{\vec{T}} &= \kappa \vec{N} \\ \dot{\vec{N}} &= -\kappa \vec{T} + \tau \vec{B} \\ \dot{\vec{B}} &= -\tau \vec{N}\end{aligned}$$

where  $\kappa(s)$  is the curvature of , and  $\tau(s)$  is the torsion. Torsion is the rate of rotation around the tangent, and curvature is the rate of rotation around the binormal. The coefficients on the right side form the matrix

$$\mathcal{R} = \begin{pmatrix} 0 & \kappa & 0 \\ -\kappa & 0 & \tau \\ 0 & -\tau & 0 \end{pmatrix}.$$

Multiplication by the matrix  $\mathcal{R}$  can be replaced by a vector product with the Darboux vector

$$\vec{\Omega} = \tau \vec{T} + \kappa \vec{B}$$

which is the rotational velocity of the moving trihedron. The velocity of the origin is given by  $\dot{\vec{t}} = \vec{T}$ . All derivatives are taken with respect to  $s$ . The velocity of the environment point  $\vec{r}_e$  in the moving trihedron coordinate system is then given by

$$\dot{\vec{r}}_e = -\vec{T} - (\tau \ 0 \ \kappa)^T \times \vec{r}_e. \quad (2)$$

If  $\tau = 0$ , , is a plane curve and  $\vec{B}$  is a constant vector. If the relative position of the camera frame (chosen with the nodal point of the camera as the origin) and the moving trihedron remains constant, the resulting motion is called *Frenet-Serret motion* [3]. If the observer additionally rotates at the same time around an axis passing through the nodal point  $O$ , the resulting motion is the most general motion possible. If, instead of using arc length  $s$  as a parameter, time  $t$  is used, the rotational velocity  $\vec{\Omega}$  and translational velocity  $\vec{T}$  are scaled by the speed  $v = ds/dt$  of the nodal point  $O$ . In that case the equation of motion becomes

$$\dot{\vec{r}}_e = -\vec{T} v - [(\tau \ 0 \ \kappa)^T \times \vec{r}_e] v.$$

All derivatives are taken with respect to time.

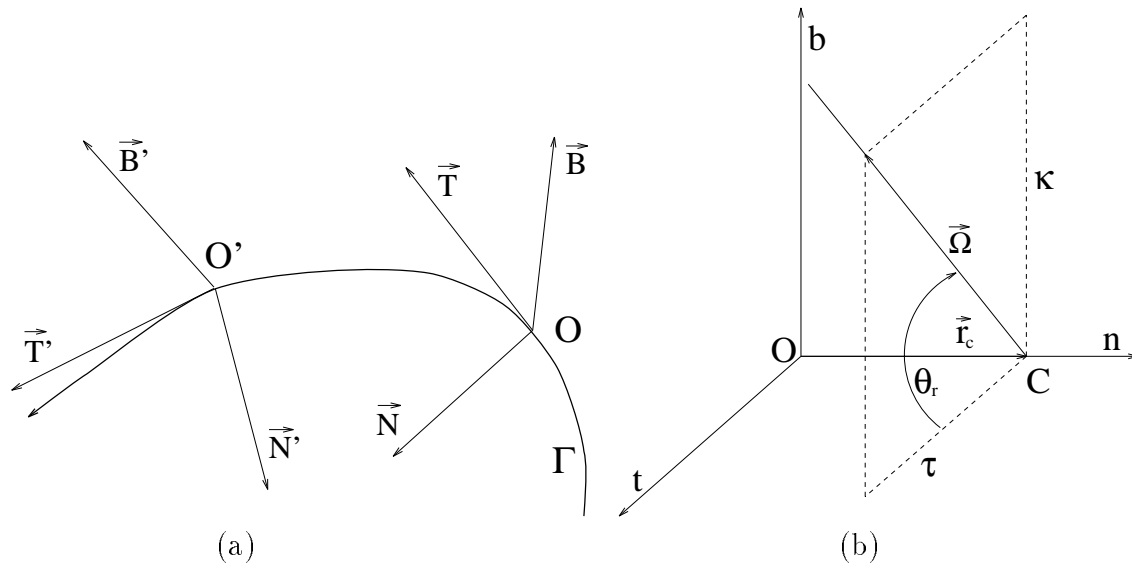


Figure 1: (a) The natural trihedron moves along the path  $\Gamma$ . Coordinate unit vectors  $(\vec{T}, \vec{N}, \vec{B})$  at  $O$  become  $(\vec{T}', \vec{N}', \vec{B}')$  at  $O'$ . (b) The screw axis passes through the point  $C$  on the principal normal.

The screw motion parameters for Frenet-Serret motion are

$$\vec{r}_c = \left(0 \quad \frac{\kappa}{\kappa^2 + \tau^2} \quad 0\right)^T + \mu(\tau \quad 0 \quad \kappa)^T \quad (3)$$

$$\sigma = \frac{\tau}{\kappa^2 + \tau^2} \quad (4)$$

where  $\mu$  is an arbitrary scalar. If  $\mu = 0$  then  $\vec{r}_c$  is the point where the screw axis pierces the osculating plane of  $\Gamma$ , (see Figure 1b).

### 3 The Imaging Model

Consider a sphere with the nodal point  $O$  of the camera at its center and with its radius equal to the camera focal length  $f$ ; without loss of generality we can set  $f = 1$  so that the sphere is a unit sphere. This sphere will be called the *image egosphere (IE)* [1]. Consider a Cartesian coordinate system  $Otnb$  with origin  $O$  and with positive  $t$ -axis pointing from  $O$  to the north pole  $N$  of the *IE*. Let  $\Pi$  be the plane tangent to the *IE* at  $N$ . If the image of the scene is obtained through plane perspective projection, the image surface is  $\Pi$ ; if the image is obtained through spherical projection, the image surface is the *IE* (see Figure 2). It is shown in [9] how the spherical projection image is related to the perspective projection

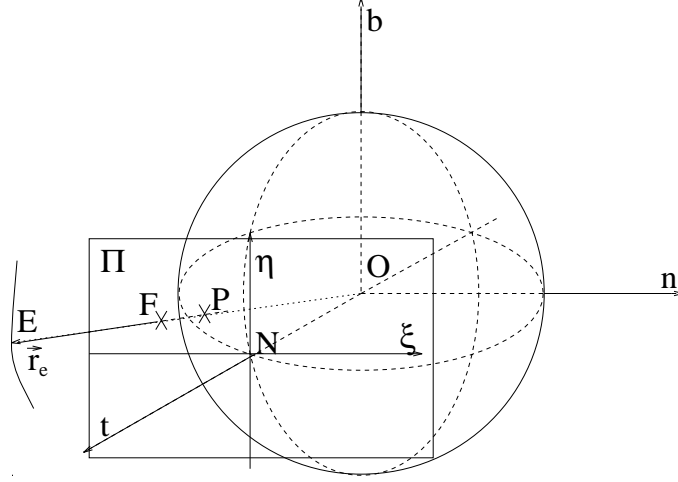


Figure 2: The perspective projection image of scene point  $E = (t, n, b)$  is  $F = (1, \xi, \eta) = (1, n/t, b/t)$ ; the spherical projection image of  $E$  is  $P = (t/R, n/R, b/R) = (1/R_t, \xi/R_t, \eta/R_t)$  where  $R = \|\vec{r}_e\|$  and  $R_t = R/t$ .

image; the perspective projection of a scene point  $(t, n, b)$  is  $(1, \xi, \eta) = (1, n/t, b/t)$  and its spherical projection is  $(t/R, n/R, b/R) = (1/R_t, \xi/R_t, \eta/R_t)$ , where  $R = \sqrt{t^2 + n^2 + b^2}$  and  $R_t = R/t = \sqrt{1 + \xi^2 + \eta^2}$ .

Let  $\vec{r}_e$  be a scene point, and let  $R = \|\vec{r}_e\|$  be its distance from  $O$ . Then  $\vec{r}_e/R$  is a unit vector  $\vec{r}$  from  $O$  to the surface of the  $IE$ . In other words, projection onto the  $IE$  satisfies the equation

$$\frac{\vec{r}}{f} = \vec{r} = \frac{\vec{r}_e}{R}. \quad (5)$$

A scene point is defined either by a vector  $\vec{r}_e = (t \ n \ b)^T$  in Cartesian coordinates, or by a triple  $(\rho, \theta, \varphi)$ , where  $\rho = R$ , in spherical coordinates (see Figure 3). The relationship between the spherical and the Cartesian coordinates is defined by

$$t = \rho \cos \theta, \quad n = \rho \cos \varphi \sin \theta, \quad b = \rho \sin \varphi \sin \theta, \quad \theta \in [0, \pi], \quad \varphi \in [0, 2\pi], \quad \rho \in [0, \infty).$$

It is also convenient to introduce a system of orthogonal unit vectors  $\vec{e}_\rho, \vec{e}_\theta, \vec{e}_\varphi$  as shown in Figure 3; note that  $\vec{r}_e = \rho \vec{e}_\rho$ , so that  $\vec{r}$  (in equation (5)) is equal to  $\vec{e}_\rho$  and it has spherical coordinates  $(1, \theta, \varphi)$ .

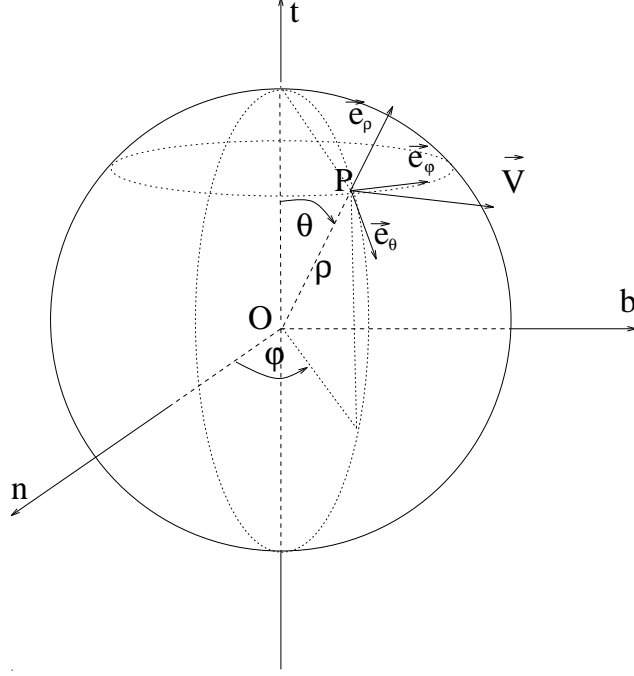


Figure 3: The point  $P = (t, n, b)$  has spherical coordinates  $(\rho, \theta, \varphi)$  where  $\theta$  is the angle between the line  $OP$  and the  $t$ -axis,  $\varphi$  is the angle between the  $n$ -axis and the projection of  $OP$  onto the normal plane  $nOb$ , and  $\rho$  is the length of  $OP$ . The unit vectors associated with the spherical coordinate system are  $\vec{e}_\theta$ ,  $\vec{e}_\varphi$ , and  $\vec{e}_\rho$ .

### 3.1 The Motion Field and the Optical Flow Field

The instantaneous velocity of the image point  $\vec{r}$  on the  $IE$  is obtained by taking derivatives of both sides of (5) with respect to time, and using (5) and (1) as well as  $\dot{R} = \dot{r}_e \cdot \vec{r}_e / R$ :

$$\dot{\vec{r}} = \frac{R \dot{\vec{r}}_e - \dot{R} \vec{r}_e}{R^2} = \frac{1}{R} [-\vec{t} + \vec{r}(\vec{t} \cdot \vec{r})] - \vec{\Omega} \times \vec{r}.$$

The first term on the r.h.s. is the *translational motion field*  $\dot{\vec{r}}_t$ , and the second term is the *rotational motion field*  $\dot{\vec{r}}_\omega$ . Note that  $\dot{\vec{r}}$  is equal to  $(\dot{\vec{r}}_e)^\perp / R$ , where  $(\dot{\vec{r}}_e)^\perp$  is the component of  $(\dot{\vec{r}}_e)$  perpendicular to  $\vec{r}_e$ .

We can obtain simple expressions for  $\dot{\vec{r}}_t$  and  $\dot{\vec{r}}_\omega$  in spherical coordinates by using a coordinate system  $Otnb$  in which the  $t$ -axis is parallel to  $\vec{t}$  and  $\vec{\Omega}$  is parallel to the rectifying plane  $tOb$ , so that  $\vec{t} = \vec{T}$  and  $\vec{\Omega} = (\tau \ 0 \ \kappa)^T$ . In spherical coordinates,  $\dot{\vec{r}}_t$  and  $\dot{\vec{r}}_\omega$  then become

$$\dot{\vec{r}}_t = \frac{1}{\rho} \sin \theta \vec{e}_\theta, \quad \dot{\vec{r}}_\omega = -\kappa \cos \varphi \vec{e}_\theta + (\kappa \cos \theta \sin \varphi - \tau \sin \theta) \vec{e}_\varphi. \quad (6)$$

If we choose a direction  $\vec{n} = \cos \alpha \vec{e}_\theta + \sin \alpha \vec{e}_\varphi$  in the image (at the point  $\vec{r}$ ) and call it the normal direction, then the *normal motion field* at  $\vec{r}$  is

$$\dot{\vec{r}}_n = (\dot{\vec{r}} \cdot \vec{n})\vec{n} = \left[ \left( \frac{1}{\rho} \sin \theta - \kappa \cos \varphi \right) \cos \alpha + (\kappa \cos \theta \sin \varphi - \tau \sin \theta) \sin \alpha \right] \vec{n}. \quad (7)$$

$\vec{n}$  can be chosen in various ways; the usual choice (as we shall now see) is the direction of the image intensity gradient.

Let  $I(\theta, \varphi, t)$  be the image intensity function. The image gradient in spherical coordinates is given by

$$\nabla I = \frac{\partial I}{\partial \theta} \vec{e}_\theta + \frac{1}{\sin \theta} \frac{\partial I}{\partial \varphi} \vec{e}_\varphi.$$

The time derivative of  $I$  can be written in terms of  $\nabla I$  as

$$\frac{dI}{dt} = \frac{\partial I}{\partial \theta} \frac{d\theta}{dt} + \frac{\partial I}{\partial \varphi} \frac{d\varphi}{dt} + \frac{\partial I}{\partial t} = \nabla I \cdot \vec{u} + I_t$$

where  $\vec{u} = \dot{\theta} \vec{e}_\theta + \sin \theta \dot{\varphi} \vec{e}_\varphi$ . This last expression is simply the velocity of a point on the surface of the  $IE$ , expressed in spherical coordinates.

It is usually assumed that  $dI/dt = 0$ , i.e. that the image intensity does not vary with time [8]. It follows that  $\nabla I \cdot \vec{u} = -I_t$ ; in this expression,  $\vec{u}$  is called the *optical flow*. If we choose the normal direction  $\vec{n}$  to be the image gradient direction  $\nabla I / \|\nabla I\|$ , we then have

$$\vec{u}_n = (\vec{u} \cdot \vec{n})\vec{n} = \frac{-I_t \nabla I}{\|\nabla I\|^2} \quad (8)$$

where  $\vec{u}_n$  is called the *normal flow*.

It was shown in [17] that for this choice of  $\vec{n}$  we have  $\dot{\vec{r}}_n \approx \vec{u}_n$  when  $\|\nabla I\|$  is large. Equations (7) and (8) thus provide an approximate relationship between the 3-D motion and the image derivatives. We will use this approximation later in this paper.

## 4 Velocity patterns

We investigate the patterns of the projected motion field (or velocity patterns) induced by an observer moving through the environment. The motion of the observer is Frenet–Serret motion. The patterns of the projected motion field on the surface of the  $IE$  depend on the

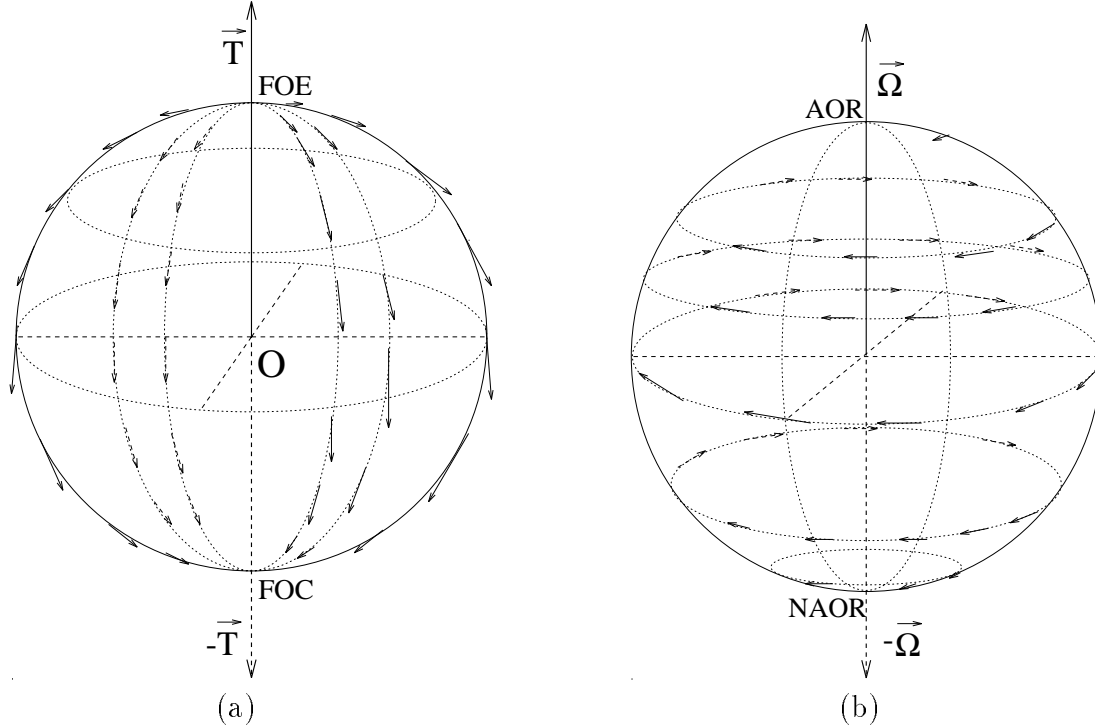


Figure 4: (a) The optical flow vectors are tangent to great circles (meridians). The two singular points (the *FOE* and the *FOC*) at which the optical flow is zero correspond to the points where  $\vec{T}$  and  $-\vec{T}$  pierce the image egosphere. (b) The optical flow vectors are tangent to the parallels (the circles centered on the axis joining the north and south poles). The two singular points (the *AOR* and the *NAOR*) at which the optical flow is zero correspond to the points where  $\vec{\Omega}$  and  $-\vec{\Omega}$  pierce the image egosphere.

torsion and curvature of the observer’s path and the range  $\rho = \rho(\theta, \varphi)$ . If the motion is either pure translation or pure rotation the velocity pattern is very simple (see Figure 4). In the case of Frenet-Serret motion the patterns change between two “pure” cases as the range changes. We will first analyze the cases in which either torsion  $\tau$  or curvature  $\kappa$  is zero, and then we will proceed to the case of general Frenet–Serret motion.

#### 4.1 Motion in a Plane

When torsion  $\tau = 0$  the observer is moving in the osculating plane. The observed velocity pattern depends on the curvature  $\kappa$  and range  $\rho(\theta, \varphi)$ . The 3–D velocity is defined by

$$\dot{r}_e^{\rightarrow} = - (0 \ 0 \ \kappa)^T \times (r_e^{\rightarrow} - (0 \ \rho_c \ 0)^T)$$

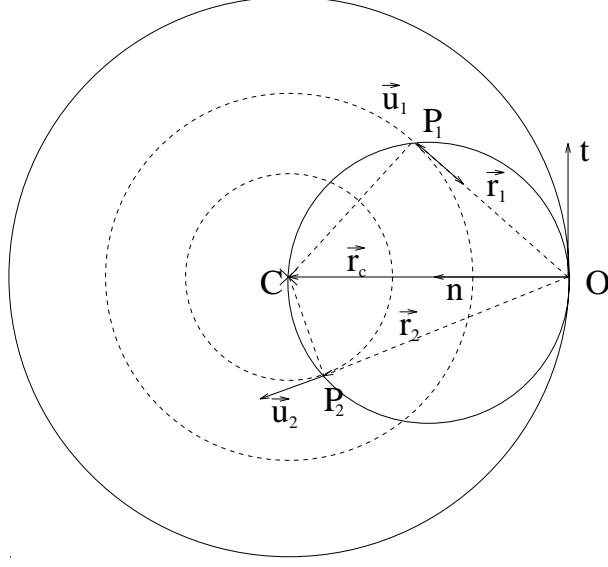


Figure 5: The singular points of type I all lie in the osculating plane on the circle which passes both through the origin  $O$  and the point  $C$  at which the screw axis pierces the plane. The 3-D velocity vectors are tangents to circles centered at  $C$ . The optical flow vectors are zero for the points  $P_i$  whose position vectors  $\vec{r}_i$  are parallel to the 3-D velocities  $\vec{u}_i$ .

where  $\rho_c = \kappa^{-1}$  is the *radius of curvature* of the path , , and the projected motion field (on the  $IE$ ) is defined by

$$\dot{\vec{r}} = \frac{1}{\rho} \sin \theta \vec{e}_\theta - \kappa \cos \varphi \vec{e}_\theta + \kappa \cos \theta \sin \varphi \vec{e}_\varphi.$$

The 3-D velocity vectors are tangents to cylinders whose axes are the same as the screw axis. This axis is parallel to the binormal  $\vec{B}$  and passes through  $\vec{r}_c = (0 \ \rho_c \ 0)^T$  (see Figure 1b). The surface  $\rho(\theta, \varphi)$  intersects the 3-D velocity field and the components of the velocity vectors orthogonal to the viewing directions are projected onto the  $IE$ . Points at which the projected motion field is zero are singular points. In the case of pure rotational (or pure translational) motion there are two singular points (see Figure 4). In the case of plane Frenet-Serret motion the situation is different. Looking at the 3-D velocity field and using the geometry of the projection on the  $IE$  we can see that the number of singular points can be infinite.

The projected motion field is zero iff  $\dot{\vec{r}} = \vec{0}$ . This is true when

$$\frac{1}{\rho} \sin \theta = \kappa \cos \varphi, \quad \kappa \cos \theta \sin \varphi = 0.$$

From the second equation we have either (i)  $\cos \theta = 0$  ( $\theta = \pi/2$ ), or (ii)  $\sin \varphi = 0$  ( $\varphi = 0, \pi$ ).

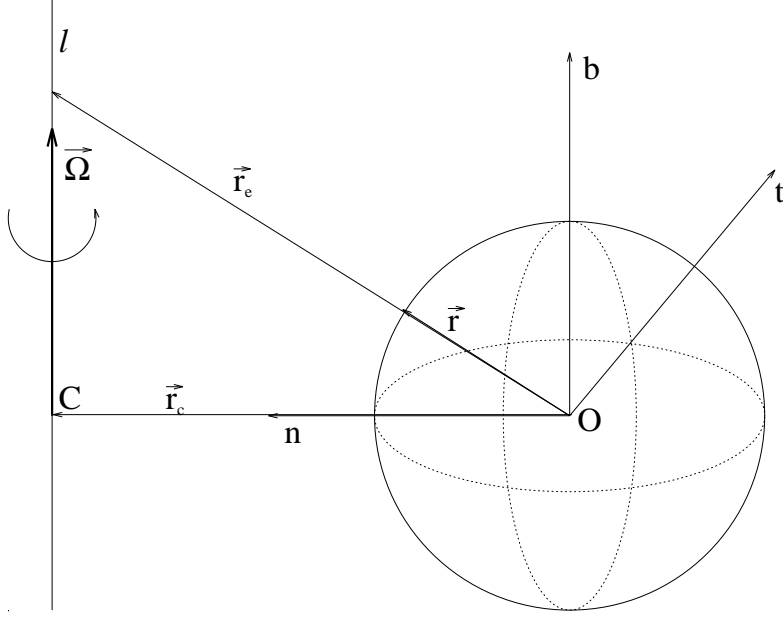


Figure 6: The singular points of type II all lie on the screw axis  $l$ . The world point  $\vec{r}_e$  whose velocity is zero projects on the  $IE$  at the point  $\vec{r}$ .

It is easy to see that only  $\varphi = 0$  is possible if we assume that  $\kappa > 0$  (which can be assured by the choice of coordinate system). If  $\varphi = 0$  we get the angle

$$\theta_0 = \arcsin \frac{\rho}{\rho_c} \quad (9)$$

for the singular point. This kind of singular point exists iff  $\rho < \rho_c$ . We will refer to this type of singular point as a *singular point of type I*. If  $\cos \theta = 0$  ( $\theta = \pi/2$ ) we have the angle

$$\varphi_0 = \arccos \frac{\rho_c}{\rho} \quad (10)$$

for the singular point. This kind of singular point exists iff  $\rho > \rho_c$ . We will refer to this type of singular point as a *singular point of type II*. For the singular points of type I the observer looks at the point whose 3-D velocity is parallel to the viewing direction, so that its projected velocity is zero. These are points where the viewing directions are tangent to circles centered at  $\vec{r}_c$ , and they lie on the circle in the osculating plane which passes through the nodal point of the observer and through the point  $\vec{r}_c$  on the screw axis. The angle between the viewing direction and the radius of the circle centered at  $\vec{r}_c$  to which the viewing direction is tangent is  $90^\circ$ . Also, the radius of curvature is the base of every right triangle which has as its other two sides the viewing direction and the radius of the circle centered at  $\vec{r}_c$ . Therefore,

all singular points in the osculating plane lie on the circle whose diameter is the radius of curvature. This circle (see Figure 5) has been called the zero-flow circle (*ZFC*) [13]. In the image these points lie on the great circle in which the osculating plane intersects the *IE*. For singular points of type II the observer looks at a point which lies on the screw axis; the 3-D velocity and therefore the projected velocity is zero. In the image these points lie on the great circle which is cut by the normal plane on the *IE* (see Figure 6). It is obvious that in order to have a singular point both the viewing direction and the range must be appropriate.

At any given point on the path, there are two circles which lie in the osculating plane and pass through  $O$ . The osculating circle (*OC*) has radius  $\rho_c$  and is centered on the screw axis. The *ZFC* has the radius  $\rho_c/2$ , and is always inside the *OC*. When  $\kappa \rightarrow 0$ ,  $\rho_c \rightarrow \infty$  the radii of both circles grow. When  $\kappa = 0$  the screw axis moves to infinity and both circles degenerate into a line ( $\gamma$  is locally a line). In that case we have pure translational (straight line) motion. When  $\kappa \rightarrow \infty$  then  $\rho_c \rightarrow 0$ , the radii of both circles get smaller; finally when the binormal and the screw axis merge we have pure rotational motion. This suggests that the ratio of range and radius of curvature determines the “dominance” of rotation or translation.

The equation  $\rho(\theta, \varphi) = \rho_0$  represents a sphere  $\Sigma$  of radius  $\rho_0$  with the center at the nodal point  $O$  of the camera. The projected motion field is equal to the component of the 3-D velocity tangent to  $\Sigma$  divided by the range  $\rho_0$ . If  $\rho_0 < \rho_c$  we will get a field with two singular points of type I. These points are the projections on the *IE* of the points which are the intersections of  $\Sigma$  with the *ZFC*. Because of the orthogonality of the 3-D velocity and the sphere  $\Sigma$  the motion field pattern in the neighborhood of the singular points is similar to the pattern around the *FOE* and the *FOC*. The projected motion field pattern looks as if the motion were pure translation and the space were “curved” around the screw axis. The smaller the ratio  $\rho_0/\rho_c$  the less curved the space. If we visualize the *IE* for pure translational motion with meridians joining the two poles (the *FOE* and the *FOC*) the curving will move the poles for the angle  $\theta_0$  towards the normal and stretch or shorten the meridians accordingly. When  $\rho_0$  grows the distance between the poles (singular points) becomes smaller until only one singular point is left. This happens when  $\rho_0 = \rho_c$  (when one is looking at the point  $\vec{r}_c$  on the

screw axis). When the radius of  $\Sigma$  grows and  $\rho_0 > \rho$ , the singular points are the projections of the points of intersection of the screw axis and  $\Sigma$ . As a result the projected motion field around the singular points will look like a pure rotational field. The rest of the field will look as if the space were curved by bending the binormal. As the radius of  $\Sigma$  grows this bending will appear to decrease until the projected motion field looks as if the motion were pure rotation. From the argument presented here we see that for constant range the pattern depends on the ratio  $\rho_0/\rho_c$ . If the ratio is less than unity the pattern looks like translation and for a ratio bigger than unity the pattern looks like pure rotation. This similarity is greater near the singular points and smaller away from them. Also, the pattern looks more “pure” when the ratio is not close to unity. Of course if the range is not constant the pattern will be different, but it will always be a combination of the patterns described here.

## 4.2 Rotation Around the Heading Direction

When curvature  $\kappa = 0$  the observer is moving along a straight line and possibly rotating around the heading direction. The observed velocity pattern depends on the torsion  $\tau$  and range  $\rho(\theta, \varphi)$ . The 3-D velocity is defined by

$$\dot{r}_e = -(1 \ 0 \ 0)^T - (\tau \ 0 \ 0)^T \times \vec{r}_e.$$

The projected motion field (on the  $IE$ ) is defined by

$$\dot{r} = \frac{1}{\rho} \sin \theta \vec{e}_\theta - \tau \sin \theta \vec{e}_\varphi.$$

The 3-D velocity vectors  $\dot{r}_e$  are tangents to helices which lie on cylinders whose axis is the heading direction (which is at the same time the screw axis and is parallel to the tangent  $\vec{T}$ ). The surface  $\rho(\theta, \varphi)$  intersects the 3-D velocity field and the components of the velocity vectors orthogonal to the viewing direction get projected onto the  $IE$ . There are two singular points which are the same as in the case of translation or rotation. The angle  $\alpha$  between the projected motion vectors and the meridians connecting the singular points (the poles of the  $IE$ ) is given by

$$\alpha = -\arctan \tau \rho = -\arctan \frac{\rho}{\sigma} \quad (11)$$

where  $\sigma = \tau^{-1}$  is the pitch of screw motion (see equation (4)). It is clear that the pattern depends on the ratio  $\rho/\sigma$ . When it is unity we have  $|\alpha| = \pi/4$  and neither translation nor rotation dominates. When the product is small we have  $\rho < \sigma$  ( $|\alpha| < \pi/4$ ) and translation dominates, and when  $\rho > \sigma$  ( $|\alpha| > \pi/4$ ) rotation is dominant. When  $\alpha = 0$  we have pure translation, and for  $\alpha = \pm\pi/2$  we have pure rotation.

### 4.3 General Frenet-Serret motion

The path  $\gamma$  has the osculating helix ( $OH$ ) whose axis is the screw axis and whose radius is  $\rho_c = \kappa/(\kappa^2 + \tau^2)$ . If the curvature  $\kappa$  and torsion  $\tau$  remained constant then  $OH$  and  $\gamma$  would be the same. All points in the world move along tangents to helices whose axes are the screw axis. The torsion and the curvature differ for all the helices which do not lie on the same cylinder. Let  $\Xi$  be the plane to which the screw axis is orthogonal and in which the nodal point  $O$  of the observer lies. The angle between the osculating plane and the screw axis is given by

$$\theta_r = \arctan \frac{\kappa}{\tau}$$

(see Figure 1b) and the angle between  $\Xi$  and the osculating plane is

$$\beta_0 = \pi/2 - \theta_r.$$

The relative size of  $\kappa$  and  $\tau$  makes one of the two cases described previously dominant. When  $\kappa \rightarrow 0$ , then  $\theta_r \rightarrow 0$  and the dominant motion will be rotation around the heading direction. When  $\tau \rightarrow 0$ , then  $\theta_r \rightarrow \pi/2$  and the dominant motion will be motion in a plane.

The rotation vector is  $\vec{\Omega} = (\tau \ 0 \ \kappa)^T$  and its norm is equal to the total curvature of the path  $\gamma$ , given by  $\lambda = \sqrt{\kappa^2 + \tau^2}$ . The pitch of the screw motion is  $\sigma = \tau/\lambda^2$  and the component of motion along the screw axis is  $\sigma\vec{\Omega}$ . Because  $\sigma \neq 0$  there are no points in the world whose 3-D velocity is zero. Therefore, the points where the projected motion field is zero are those points where the 3-D velocity vectors are parallel to the viewing direction. Consider a 3-D velocity vector  $\dot{\vec{r}}_e$  at the point  $W$  with position vector  $\vec{r}_e$  such that  $\dot{\vec{r}}_e$  and  $\vec{r}_e$  are parallel (see Figure 7). The 3-D velocity  $\dot{\vec{r}}_e$  (at the point  $W$ ) has two components which are orthogonal: (i) the component  $\vec{u}_r$  parallel to  $\Xi$  with norm  $r\lambda$ , where  $r$  is the distance

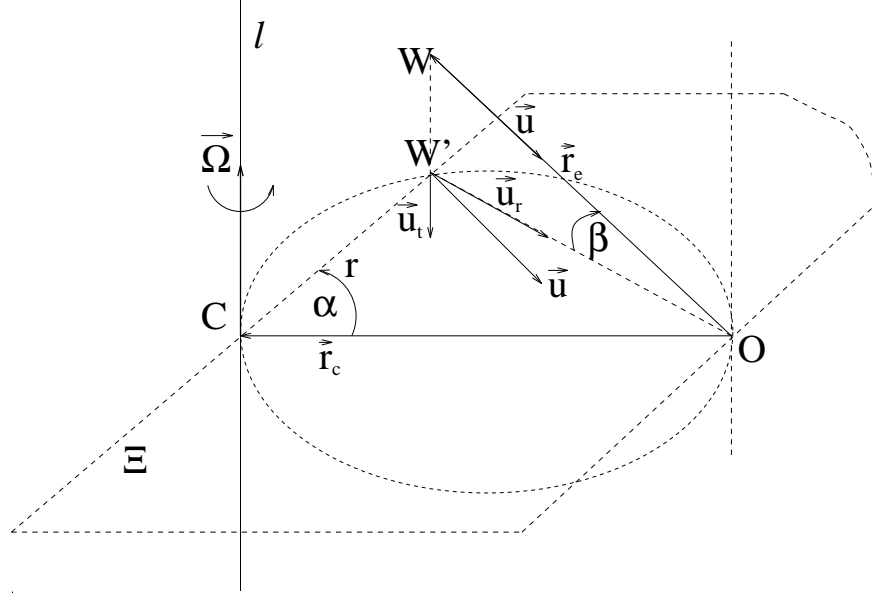


Figure 7:  $\vec{r}_e$  and  $\vec{u} = \dot{\vec{r}}_e$  are parallel at  $W$ . The projection of  $W$  on  $\Xi$  (the plane orthogonal to the screw axis  $l$ ) lies on the circle on  $\Xi$  which is tangent to the screw axis and passes through the focal point  $O$ .

between  $W$  and the screw axis, and (ii) the component  $\vec{u}_t$  orthogonal to  $\Xi$  (parallel to the screw axis) with norm  $\sigma\lambda$ . The projection of  $W$  on  $\Xi$  is point  $W'$  (the line joining  $W$  and  $W'$  is orthogonal to  $\Xi$ ). The angle between  $\vec{r}_e$  and  $\Xi$  is given by

$$\beta = \pm \arctan \frac{\sigma}{r} \quad (12)$$

and is a two valued function of  $r$ . We will show that  $\beta(r)$  projects into a circle on  $\Xi$ . The 3-D velocity at  $W'$  is the same as at  $W$ ; therefore the component of 3-D velocity at  $W'$  parallel to  $\Xi$  is equal to  $\vec{u}_r$ . But  $\vec{u}_r$  is orthogonal to the line joining  $C$  and  $W'$  and parallel to line  $OW'$  which means that the two lines at  $W'$  form a right angle. But then all possible positions for  $W'$  on  $\Xi$  lie on the circle whose diameter is  $\rho_c$  and which touches both the screw axis and the focal point of the observer  $O$ . This circle is projection of the  $OH$  onto  $\Xi$ . If the angle between line  $CW'$  and  $\vec{r}_c$  is  $\alpha$  we have

$$\rho_c \cos \alpha = r, \quad \rho_c \sin \alpha = \rho \cos \beta.$$

For any  $\rho$  there are two points for which the 3-D velocity and the viewing direction are parallel: one for which  $\vec{r}_e \dot{\vec{r}}_e > 0$  (positive  $\beta$ ) and one for which  $\vec{r}_e \dot{\vec{r}}_e < 0$  (negative  $\beta$ ). For each of these points we have a unique  $\alpha$  and  $r$ . One singular point is “above”  $\Xi$  and on the

right side of the line  $OC$ ; the other is “below”  $\Xi$  and on the left side of  $OC$ . As  $r$  changes over the range  $(\rho_c, 0)$ ,  $\rho$  changes over the range  $(0, \infty)$ ,  $\beta$  changes over the range  $(\beta_0, \pi/2)$  ( $(-\beta_0, -\pi/2)$  for negative  $\beta$ ), and  $\alpha$  changes over the range  $(0, \pi/2)$  ( $(0, -\pi/2)$  for negative  $\beta$ ). The geometric loci of the singular points are spiral-like curves which lie on the  $ZFC$  and whose asymptote is the screw axis.

If we assume that the components of image velocity tangent to the meridians and parallels are zero we get

$$\frac{1}{\rho} \sin \theta - \kappa \cos \varphi = 0$$

and

$$\kappa \cos \theta \sin \varphi - \tau \sin \theta = 0.$$

If  $\kappa = 0$  and  $\tau = 0$  we have pure translational motion. The two singular points correspond to the  $FOE$  and the  $FOC$ . When  $\rho \rightarrow \infty$  rotational motion becomes dominant. There are two singular points which are the same as the  $AOR$  and the  $NAOR$ . Their positions in  $(\theta, \varphi)$  coordinates are  $(\theta_r, \pi/2)$  and  $(\pi - \theta_r, -\pi/2)$ , respectively. For any other triple  $(\rho, \kappa, \tau)$  there are two singular points which are the solutions of the above equations. All singular points for a fixed  $(\kappa, \tau)$  lie on the curves  $(FOE) - (AOR)$  and  $(FOC) - (NAOR)$  which can be determined as functions of  $\rho$ . From the continuity of the curves on which the singular points lie in 3-D, as well as the uniqueness of the singular points for any  $\rho$ , we can see that the loci of the singular points on the  $IE$  are continuous curves. We have

$$\tan \theta_r \sin \varphi = \tan \theta$$

which means that for smaller  $\theta$  we must have smaller  $\varphi$ . From the first equation we have

$$\frac{\sin \theta}{\cos \varphi} = \rho \kappa$$

which shows that as  $\rho$  gets smaller both  $\theta$  and  $\varphi$  get smaller, and as  $\rho$  grows they both grow. But as  $\rho$  gets smaller the singular point gets closer to the  $FOE$  and as it grows it gets closer to the  $AOR$ .

The equation  $\rho(\theta, \varphi) = \rho_0$  represents a sphere  $\Sigma$  of radius  $\rho_0$  with the center at the nodal point of the camera. If  $\rho_0$  is the range the projected motion field can be computed from the

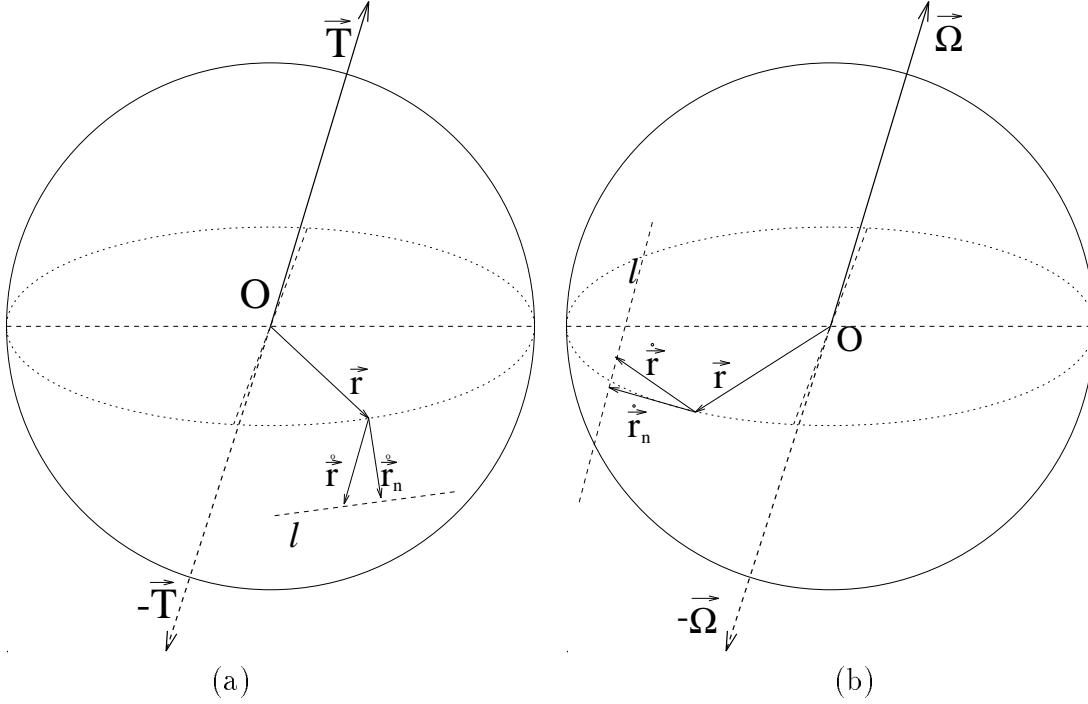


Figure 8: (a) All the points on the hemisphere to which  $\vec{T}$  belongs (the hemisphere “behind”  $\vec{r}_n$ ) are candidates for the *FOE*. (b) All the points on the hemisphere “to the right” of  $\vec{r}_n$  are candidates for the *AOR*.

intersection of the sphere  $\Sigma$  and the 3-D velocity field. If  $\rho_0 \ll \rho_c$  (this is possible only if  $\rho_c \gg 1$ ) the projected motion field looks very similar to a pure translational field and we say that the *translation is dominant*. If  $\rho_0 \gg \rho_c$  the velocity pattern is very similar to a pure rotational field and we say that the *rotation is dominant*. As  $\rho_0$  varies over the range  $(1, \infty)$  the velocity pattern on the *IE* changes. The singular points move from the *FOE* to the *AOR* and from the *FOC* to the *NAOR*. Also the pattern in the neighborhoods of the singular points varies from pure or dominant translation to dominant or pure rotation. If the range  $\rho(\theta, \varphi)$  is not constant the resulting field will be a combination of the fields described above.

## 5 Egomotion Estimation from Normal Flow by Constraint Intersection: Pure Translation or Rotation

In the case of pure translational motion, the projected motion field has only a component parallel to  $\vec{e}_\theta$ . The projected motion field vectors are parallel to the great circles (meridians) passing through the poles and their direction is away from the north pole and towards the south pole. The corresponding vector field on the IE has two singularities; a source at the north pole called the *Focus of Expansion (FOE)* and a sink at the south pole called the *Focus of Contraction (FOC)* (see Figure 4a).

Each projected motion field vector defines a great circle on which both the FOE and the FOC lie. Therefore all the circles intersect at the FOE and the FOC. If only normal flow is available at each point the constraints on the FOE and the FOC will be different. Given the normal motion field  $\dot{\vec{r}}_n$  at  $\vec{r}$  it is clear that all possible projected motion field vectors are constrained to lie on the line  $l$  called the *flow constraint line*. But this constrains the FOE to belong to the hemisphere “behind” the great circle passing through  $\vec{r}$  and orthogonal to  $\dot{\vec{r}}_n$  (see Figure 8a). Given the point  $\vec{r}_i$  with the unit normal  $\vec{n}_i$  (the spatial gradient direction at the feature point  $\vec{r}_i$  on the *IE*) and the normal flow  $\dot{\vec{r}}_{n,i}$  the point  $\vec{r}$  is a possible FOE position iff

$$\dot{\vec{r}}_{n,i}(\vec{r} - \vec{r}_i) < 0.$$

If we substitute  $\vec{r} = \vec{T}$  the equation holds, while for  $\vec{r} = -\vec{T}$  it does not. This means that the FOE satisfies the inequality while the FOC does not. The inequality written in this form holds both for spherical and perspective projections, although for spherical projection it can be written in a simpler form, namely

$$\dot{\vec{r}}_{n,i} \cdot \vec{r} < 0 \tag{13}$$

since  $\dot{\vec{r}}_{n,i} \cdot \vec{r}_i = 0$ . For  $\vec{r} = \vec{T}$  we obtain

$$\dot{\vec{r}}_{n,i} \cdot \vec{T} = (\dot{\vec{r}}_t \cdot \vec{n}_i)(\vec{n}_i \cdot \vec{T}) = \frac{1}{\rho} [-\vec{T} + \vec{r}_i(\vec{r}_i \cdot \vec{T})] \vec{n}_i(\vec{n}_i \cdot \vec{T}) = -\frac{1}{\rho}(\vec{T} \cdot \vec{n}_i)^2 < 0$$

since  $\vec{r}_i \cdot \vec{n}_i = 0$ .

In the case of pure rotational motion the motion field vectors are tangent to small circles (parallels) whose centers are the two poles of the IE and which are orthogonal to the meridians passing through these poles. The poles (which are singular points of type center) correspond

to the intersections of the IE and the axis of rotation. The north pole will be called the *axis of rotation (AOR)* and the south pole will be called the *negative axis of rotation (NAOR)* (see Figure 4b). Given the point  $\vec{r}_i$  with the normal flow  $\dot{\vec{r}}_{n,i}$  the point  $\vec{r}$  is a possible *AOR* position iff

$$(\vec{r}_i \times \dot{\vec{r}}_{n,i})(\vec{r} - \vec{r}_i) < 0.$$

The inequality written in this form holds for both spherical and perspective projection, although for spherical projection it can be written in a simpler form, namely

$$(\vec{r}_i \times \dot{\vec{r}}_{n,i})\vec{r} < 0 \tag{14}$$

since  $\vec{r}_i$  appears twice in the mixed vector product. If we set  $\vec{r} = \vec{\Omega}$  the equation holds, while for  $\vec{r} = -\vec{\Omega}$  it does not. But this means that the *AOR* satisfies the inequality while the *NAOR* does not. For  $\vec{r} = \vec{\Omega}$  we obtain

$$(\vec{r}_i \times \dot{\vec{r}}_{n,i})\vec{\Omega} = [\vec{r}_i \times \vec{n}_i(\dot{\vec{r}}_{\omega} \cdot \vec{n}_i)] \vec{\Omega} = [(\vec{r}_i \times \vec{n}_i)\vec{\Omega}][(-\vec{\Omega} \times \vec{r}_i)\vec{n}_i] = -[(\vec{r}_i \times \vec{n}_i)\vec{\Omega}]^2 < 0$$

because of the cyclical nature of the triple vector product. It is also obvious that the result would be positive for  $\vec{r} = -\vec{\Omega}$ .

In the case of pure translational (rotational) motion the constraint intersection method determines the smallest area, consistent with the normal flow field, in which the *FOE (AOR)* belongs. The constraint intersection method is implemented by counting the number of times each image egosphere point qualifies as a possible *FOE (AOR)*. The counters for some image egosphere points will represent directions which are possible *FOEs (AORs)* for the maximum numbers of normal flow vectors. These points are interpreted as possible *FOEs (AORs)* for the given normal flow field. For some tasks it may be sufficient to compute this solution set; in cases when this is not sufficient, additional constraints can be used to make the solution area smaller. Alternatively, the solution area can be represented by its center and its radius, which are interpreted as the solution and its uncertainty, respectively.

## 6 Application of the Constraint Intersection Method to Frenet-Serret Motion

In this section we investigate the performance of the constraint intersection schemes for Frenet-Serret motion. The velocity patterns depend on the curvature and torsion of the path and on the ranges of the points in the environment. The normal flow patterns depend on these and additionally on the distribution and orientation of the features. Given the normal flow  $\vec{u}_n$  for Frenet-Serret motion we want to know how useful the constraint intersection method (defined for “pure” translational or rotational motion) is for identifying the *FOE* and the *AOR* and what measures can be taken to make the constraint intersection method more reliable in practice.

Due to fundamental imaging problems the normal motion field  $\vec{r}_{n,i}$  (the projection of the 3-D velocity field on the contour normals at the feature points on the *IE*) and the normal flow  $\vec{u}_{n,i}$  at the point  $\vec{r}_i$  are not, in general, equal. However, one can assume, as in [17], that the feature points can be chosen in a way which makes the errors in computing the normal flow minimal.

Given the normal flow  $\vec{u}_{n,i}$  at a point  $\vec{r}_i$ , a point  $\vec{r}$  will be considered a candidate for the *FOE* if it satisfies inequality (13) with the computed normal flow used in place of the unknown normal motion field. The geometrical interpretation is that  $\vec{r}$  lies on the hemisphere whose border is the great circle passing through  $\vec{r}_i$  and normal to  $\vec{u}_{n,i}$  (see Figure 8a). If there is a rotational component to the motion, inequality (13) will in fact be satisfied by all  $\vec{r}$  such that

$$-\left(\frac{\vec{T}}{\rho} + \vec{\Omega} \times \vec{r}_i\right) \vec{n}_i (\vec{n}_i \cdot \vec{r}) < 0 \quad (15)$$

because  $\vec{r}_i \cdot \vec{n}_i = 0$  (the position vector is orthogonal to the gradient direction). Inequality (15) will be satisfied by all points  $\vec{r}$  which lie on the hemisphere whose border is the great circle passing through  $\vec{r}_i$  and orthogonal to  $\vec{n}_i$  and to which the unit vector in the direction  $\vec{r}_{t,i} = \vec{T}/\rho + \vec{\Omega} \times \vec{r}_i$  belongs. By writing  $\vec{\delta}_{t,i} = \vec{\Omega} \times \vec{r}_i$  we obtain  $\vec{r}_{t,i} = \vec{T}/\rho + \vec{\delta}_{t,i}$ . A constraint generated by a feature  $\vec{r}_i$  is *consistent with the actual FOE* if both  $\vec{r}_{t,i}$  and  $\vec{T}$  belong to the same hemisphere.

Given the feature point  $\vec{r}_i$  with the normal flow  $\vec{u}_{n,i}$ , a point  $\vec{r}$  is considered a candidate

for the *AOR* if it satisfies inequality (14) with the normal flow in place of the normal motion field. The geometrical interpretation is that  $\vec{r}$  lies on the hemisphere whose border is the great circle passing through  $\vec{r}_i$  and tangent to  $\vec{u}_{n,i}$ . If there is a translational component inequality (14) will be satisfied by all  $\vec{r}$  such that

$$-[(\vec{r}_i \times \vec{n}_i)\vec{r}]\left(\frac{\vec{T}}{\rho} + \vec{\Omega} \times \vec{r}_i\right)\vec{n}_i < 0.$$

Also

$$\left(\frac{\vec{T}}{\rho} \times \vec{r}_i\right) \times \vec{r}_i = -\frac{\vec{T}}{\rho} + \vec{r}_i(\vec{r}_i \cdot \frac{\vec{T}}{\rho})$$

and inequality (14) becomes

$$-[(\vec{r}_i \times \vec{n}_i)\vec{r}]\left[-\frac{\vec{T}}{\rho} \times \vec{r}_i + \vec{\Omega}\right] \times \vec{r}_i \vec{n}_i < 0. \quad (16)$$

Inequality (16) will be satisfied for all points  $\vec{r}$  which lie on the hemisphere whose border is the great circle passing through  $\vec{r}_i$  and parallel to  $\vec{n}_i$  and to which the unit vector in the direction  $\vec{r}_{\omega,i} = -(\vec{T}/\rho) \times \vec{r}_i + \vec{\Omega}$  belongs. By writing  $\vec{\delta}_{\omega,i} = -(\vec{T}/\rho) \times \vec{r}_i$  we obtain  $\vec{r}_{\omega,i} = \vec{\Omega} + \vec{\delta}_{\omega,i}$ . A constraint generated by a feature  $\vec{r}$  is *consistent with the AOR* if both  $\vec{r}_{\omega,i}$  and  $\vec{\Omega}$  belong to the same hemisphere.

## 6.1 Motion in a Plane

In this section we consider the applicability of the constraint intersection method in the special case of motion in a plane. If the observer's motion is restricted to the osculating plane then  $\tau = 0$  and in the *Otnb* frame we have  $\vec{\Omega} = (0 \ 0 \ \kappa)^T$ . Then

$$\vec{\delta}_{t,i}^\kappa = \begin{pmatrix} -\kappa \sin \theta \cos \varphi \\ \kappa \cos \theta \\ 0 \end{pmatrix}, \quad \vec{\delta}_{\omega,i}^\kappa = \begin{pmatrix} 0 \\ \rho^{-1} \sin \theta \sin \varphi \\ -\rho^{-1} \sin \theta \cos \varphi \end{pmatrix}.$$

The vectors  $\vec{\delta}_{t,i}^\kappa$  and  $\vec{r}_{t,i}$  lie in the osculating plane and the angle between the heading direction  $\vec{T}$  and  $\vec{r}_{t,i}$  varies as  $\vec{r}_i$  changes its position on the *IE*. A point  $\vec{r}$  is a candidate for the *FOE* iff it belongs to the hemisphere bounded by the great circle passing through  $\vec{r}_i$  and orthogonal to  $\vec{n}_i$ , and to which the unit vector in the direction  $\vec{r}_{t,i}$  belongs. Inequality (15) holds for the

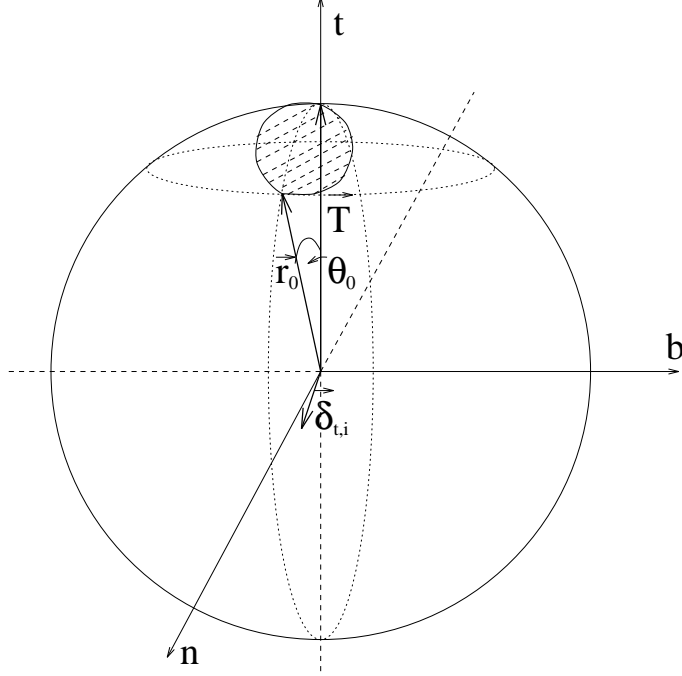


Figure 9: The inequalities are often inconsistent with the actual *FOE* for the feature points in the shaded region ( $0 \leq \theta_{t,i} \leq \theta_0$ ).  $\vec{\delta}_{t,i}$  lies in the osculating plane.

*FOE* if both  $\vec{T}$  and  $\vec{r}_{t,i}$  belong to the same hemisphere. We next develop the conditions, in terms of  $\kappa$  and  $R$ , for which this inequality will not hold for the *FOE*. The angle  $\theta_{t,i}$  between vectors  $\vec{T}$  and  $\vec{r}_{t,i}$  is given by

$$\tan \theta_{t,i} = \frac{\rho \kappa \cos \theta}{1 - \rho \kappa \sin \theta \cos \varphi}.$$

If  $\rho \kappa \leq 1$  the angle  $\theta_{t,i}$  is restricted to the range  $[0, \theta_0]$  where  $\theta_0 = \arcsin \rho \kappa$  is the angle for which the velocity field is zero (see Figure 9).  $\theta_{t,i}$  approaches its maximum,  $\theta_0$ , only at the point  $\vec{r}_0$  with  $\theta = \theta_0$ ,  $\varphi = 0$ . For  $\theta = 0$  we have  $\tan \theta_{t,i} = \sin \theta_0 = \rho \kappa$  and for  $\theta = \pi/2$  we have  $\theta_{t,i} = 0$ . We can see that  $\vec{T}$  and  $\vec{r}_{t,i}$  do not belong to the same hemisphere (inequality (15) will not hold for the *FOE*) only when the constraint circle through  $\vec{r}_i$  passes between these two vectors. This can happen if the feature point  $\vec{r}_i$  lies inside the smallest cone containing both  $\vec{T}$  and  $\vec{r}_0$ . In almost all other cases both  $\vec{T}$  and  $\vec{r}_{t,i}$  belong to the same hemisphere determined by the constraint circle. There is also a cone with similar properties close to the *FOC*. It is the smallest cone to which both  $-\vec{T}$  and the singular point  $-\vec{r}_0$  with  $(\theta = \pi - \theta_0, \varphi = \pi)$  belong. If  $\rho \kappa > 1$  the cone for which the inequality fails for the true *FOE* can be as large as the entire hemisphere with the positive direction of the normal  $\vec{N}$  as the

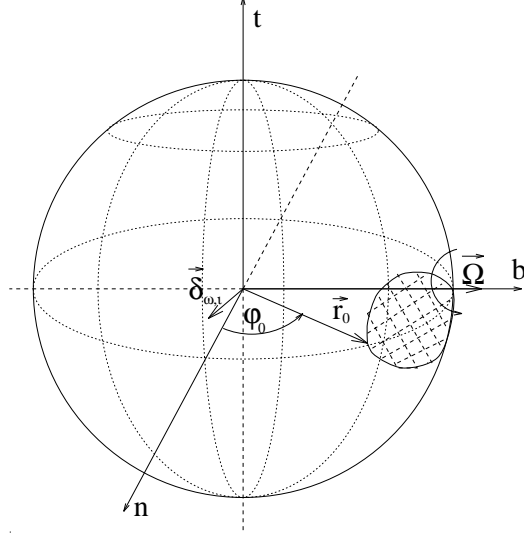


Figure 10: The inequalities are often inconsistent with the actual *AOR* for the feature points in the shaded region ( $\varphi_0 \leq \varphi_{\omega,i} \leq \pi/2$ ).  $\vec{\delta}_{\omega,i}$  lies in the normal plane.

pole. Thus, we see that it is not simply the magnitude,  $\kappa$ , of the rotation that determines the utility of the constraint integration method, but the depth-scaled rotation,  $\rho\kappa$ .

We now consider the *AOR*. The vectors  $\vec{\delta}_{\omega,i}^{\kappa}$  and  $\vec{r}_{\omega,i}$  both lie in the normal plane and the angle between the axis of rotation  $\vec{\Omega}$  and  $\vec{r}_{\omega,i}$  varies as  $\vec{r}_i$  changes its position on the *IE*. The point  $\vec{r}$  is considered a candidate for the *AOR* iff it belongs to the hemisphere bounded by the great circle passing through  $\vec{r}_i$  and parallel to  $\vec{n}_i$ , and to which the unit vector in the direction  $\vec{r}_{\omega,i}$  belongs. If inequality (16) holds for the *AOR*, then both  $\vec{\Omega}$  and  $\vec{r}_{\omega,i}$  belong to the same hemisphere. The angle  $\varphi_{\omega,i}$  between the normal  $\vec{N}$  and  $\vec{r}_{\omega,i}$  is given by

$$\cot \varphi_{\omega,i} = \frac{\sin \theta \sin \varphi}{\rho\kappa - \sin \theta \cos \varphi}.$$

The angle between  $\vec{\Omega}$  and  $\vec{r}_{\omega,i}$  is then  $\pi/2 - \varphi_{\omega,i}$ . Here,  $\rho\kappa \geq 1$ , then the angle  $\varphi_{\omega,i}$  varies over the range  $[\varphi_0, \pi/2]$ , where  $\varphi_0 = \arccos(\rho\kappa)^{-1}$  is the angle for which the velocity field is zero (see Figure 10).  $\varphi_{\omega,i}$  approaches its minimum  $\varphi_0$  only at the point  $\vec{r}_0$  with  $\varphi = \varphi_0, \theta = \pi/2$ . For  $\varphi = \pi/2$  we have  $\cot \varphi_{\omega,i} = \cos \varphi_0 = (\rho\kappa)^{-1}$  and for  $\varphi = 0$  we have  $\varphi_{\omega,i} = \pi/2$ . Again,  $\vec{\Omega}$  and  $\vec{r}_{\omega,i}$  do not belong to the same hemisphere (inequality (16) fails to hold for the *AOR*) when the constraint circle passes between these two vectors. This can happen only when the feature point  $\vec{r}_i$  is inside the smallest cone to which both  $\vec{\Omega}$  and  $\vec{r}_0$  belong. In almost all other cases both  $\vec{\Omega}$  and  $\vec{r}_{\omega,i}$  belong to the same hemisphere determined by the constraint

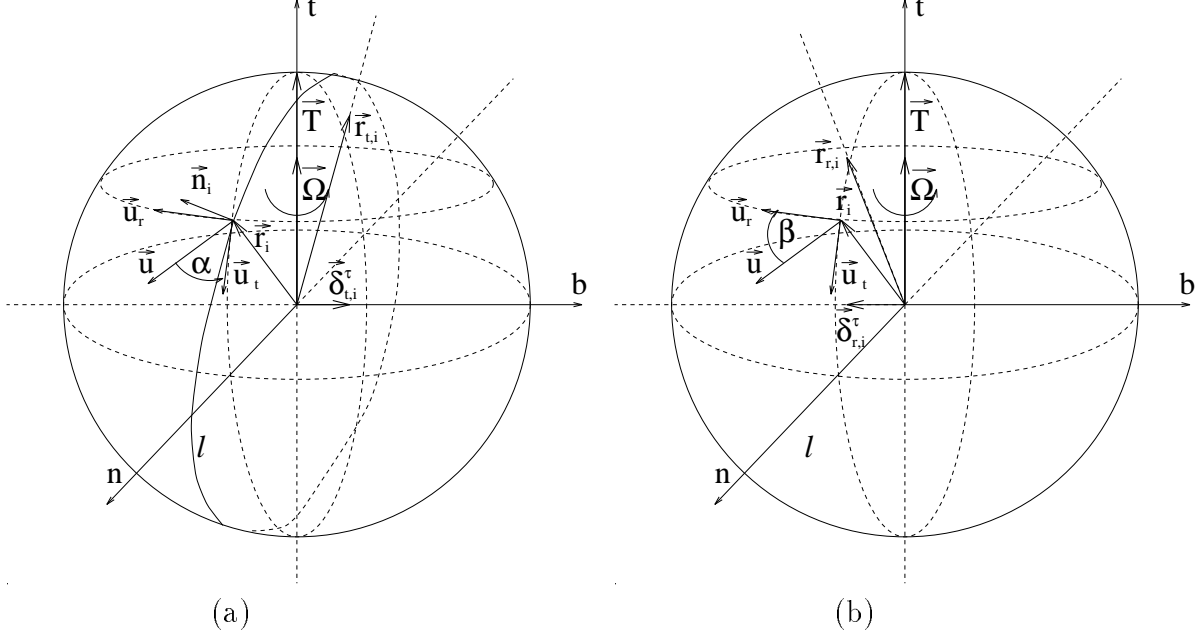


Figure 11: (a)  $\delta_{t,i}^\tau$  lies in the normal plane and  $\vec{r}_{t,i}$  lies in the plane orthogonal to the plane spanned by  $\vec{T}$  and  $\vec{r}_i$ . When the inequality is not consistent with the *FOE* the constraint circle  $l$  (orthogonal to  $\vec{n}_i$ ) passes between  $\vec{T}$  and  $\vec{r}_{t,i}$  (or between  $\vec{u}$  and  $\vec{u}_t$ ). (b)  $\delta_{\omega,i}^\tau$  lies in the normal plane and  $\vec{r}_{\omega,i}$  lies in the plane orthogonal to the plane spanned by  $\vec{\Omega}$  and  $\vec{r}_i$ .

circle. When  $\rho\kappa \leq 1$  the cone for which inequality (14) is not satisfied by the true *AOR* may be as large as the entire hemisphere with the positive direction of the normal  $\vec{N}$  as the pole.

## 6.2 Rotation Around the Heading Direction

If the observer is rotating around the heading direction the curvature  $\kappa = 0$  and in the *Otnb* we have  $\vec{\Omega} = (\tau \ 0 \ 0)^T$ . Then

$$\vec{\delta}_{t,i}^\tau = \begin{pmatrix} 0 \\ -\tau \sin \theta \sin \varphi \\ \tau \sin \theta \cos \varphi \end{pmatrix}, \quad \vec{\delta}_{\omega,i}^\tau = \vec{\delta}_{\omega,i}^\kappa.$$

Vector  $\vec{\delta}_{t,i}^\tau$  lies in the normal plane while vector  $\vec{r}_{t,i}$  lies in the plane orthogonal to the plane spanned by vectors  $\vec{T}$  and  $\vec{r}_i$  (see Figure 11a). The angle  $\theta_{t,i}$  between  $\vec{T}$  and  $\vec{r}_{t,i}$  is given by

$$\tan \theta_{t,i} = \rho\tau \sin \theta.$$

The angle between the full  $\dot{\vec{r}}$  and the translational ( $\dot{\vec{r}}_t$ ) part of the projected motion field is  $\alpha = \arctan \rho\tau$ . Vectors  $\vec{T}$  and  $\vec{r}_{t,i}$  do not belong to the same hemisphere when the angle between the feature normal  $\vec{n}_i$  and the unit vector  $\vec{e}_\theta$  belongs to the range  $[\pi/2 + \alpha, \pi/2]$  or  $[-\pi/2, -\pi/2 + \alpha]$ . From this we conclude that the ratio of the number of “bad” and “good” feature directions for constraint application is  $\alpha/\pi$ . When the ratio becomes 0.5 the outcome is completely random.

Vector  $\vec{\delta}_{\omega,i}^\tau$  lies in the normal plane while vector  $\vec{r}_{\omega,i}$  lies in the plane orthogonal to the plane spanned by vectors  $\vec{\Omega}$  and  $\vec{r}_i$  (see Figure 11b). The angle  $\theta_{\omega,i}$  between  $\vec{\Omega}$  and  $\vec{r}_{\omega,i}$  is given by

$$\tan \theta_{\omega,i} = \frac{\sin \theta}{\rho\tau}.$$

The angle between the full  $\dot{\vec{r}}$  and the rotational  $\dot{\vec{r}}_\omega$  part of the projected motion field is  $\beta = \pi/2 - \alpha$ . Vectors  $\vec{\Omega}$  and  $\vec{r}_{\omega,i}$  do not belong to the same hemisphere when the angle between the feature normal  $\vec{n}_i$  and the unit vector  $\vec{e}_\varphi$  belongs to the range  $[\pi/2, \pi/2 - \beta]$  or  $[-\pi/2 - \beta, -\pi/2]$ . From this we conclude that the ratio of the number of “bad” and “good” feature directions for constraint application is  $\beta/\pi$ .

### 6.3 General Frenet-Serret Motion

For the case when both curvature and torsion are non-zero we have in the  $Otnb$  frame  $\vec{\Omega} = (\tau \ 0 \ \kappa)^T$ . Then

$$\vec{\delta}_{t,i} = \begin{pmatrix} -\kappa \sin \theta \cos \varphi \\ \kappa \cos \theta - \tau \sin \theta \sin \varphi \\ \tau \sin \theta \cos \varphi \end{pmatrix}, \quad \vec{\delta}_{\omega,i} = \vec{\delta}_{\omega,i}^\kappa.$$

If the curvature dominates, then the effect of rotation is similar to the effect described in the previous section. Also,  $\vec{\delta}_{t,i}$ , for small  $\theta$ , is very similar to the case of motion in a plane, and for  $\theta$  close to  $\pi/2$  the effect of rotation is similar to rotation around the heading direction. We will now compute the bound on the size of the smallest cone containing  $\vec{T}$  in which the vector  $\vec{r}_{t,i}$  always lies for feature point satisfying  $\rho\kappa \leq 1$ . The size of the component of  $\vec{\delta}_{t,i}$

in the normal plane has as its extremes

$$\zeta_{1,2} = \kappa \cos \theta \pm \tau \sin \theta = \lambda \sin(\theta \pm \theta_r)$$

where  $\lambda = \sqrt{\tau^2 + \kappa^2}$  is the total curvature and  $\theta_r = \arctan(\kappa/\tau)$  (Figure 1b) is the angle between the osculating plane and the screw axis. If  $\rho\kappa \leq 1$  we have

$$\tan \theta_{t,i} \leq \frac{\rho\lambda \sin(\theta \pm \theta_r)}{1 - \rho\kappa \sin \theta \cos \varphi} \leq \frac{\rho\lambda}{1 - \rho\kappa}.$$

The constraint generated by a feature point  $\vec{r}_i$  is consistent with the *FOE* iff both  $\vec{r}_{t,i}$  and  $\vec{T}$  lie on the same side of the corresponding constraint circle. This will always be true when the entire cone defined above is on the same side of the constraint circle (the constraint may also be consistent with the *FOE* when the cone is cut by the circle). A similar analysis can be carried out for *AOR* estimation.

## 7 Increasing the Reliability of the Constraint Intersection Method

Several factors influence the reliability of egomotion estimation by constraint intersection: (i) the feature distance, (ii) the magnitude of the rotational velocity, (iii) the angle between the viewing direction and the screw axis, (iv) the size of the field of view, (v) the magnitude of the normal flow, and (vi) the distribution of features in the image.

We will first discuss the constraint intersection method for the *FOE*. It was shown that the reliability of egomotion estimation depends on the quantity  $\rho\lambda$  where  $\rho$  is the distance of the feature from the nodal point of the observer and  $\lambda$  is the total curvature of the path. By making  $\rho\lambda \ll 1$  we place an upper bound on the angle  $\theta_{t,i}$  between the direction of motion,  $\vec{T}$ , and  $\vec{r}_{t,i}$ , and guarantee, in a probabilistic sense, that most constraint hemispheres generated by image features will contain the true *FOE*. An estimate of the maximum  $\lambda$  ( $\lambda_{\max}$ ) could be obtained if the dynamics of the observer were known. (For example, in the case of ground vehicle motion the minimum turning radius can be computed for different speeds. It depends on the maximum allowable normal component  $v^2\lambda$  of the acceleration. By limiting this maximum we obtain a limit on the curvature  $\lambda_{\max}$ .) If  $\lambda_{\max}$  is known, then the maximum feature distance  $\rho_{\max}$  can be computed (and perhaps controlled, in practice, by focusing or

stereo) for which the angle  $\theta_{t,i}$  is guaranteed to be less than some predefined bound. By ensuring that the cone inside which both the direction of motion and the viewing direction lie is small relative to the field of view, we constrain the region for which the maximum number of constraints is satisfied to be small compared to the image size. Since the reliability of egomotion estimation improves for points farther away from the *FOE* (since the likelihood that their constraint hemispheres include the *FOE* increases as they move away from the *FOE*), a large field of view will ordinarily contain many points which determine constraint hemispheres consistent with the *FOE*. It is clear that a dense field with uniformly distributed directions is desirable, although the method's applicability is not limited to that case.

When the great circle passing through the feature point  $\vec{r}_i$  and orthogonal to  $\vec{u}_{n,i}$  passes "between" the *FOE* and  $\vec{r}_{t,i}$  the constraint is not consistent with the *FOE*. However it is possible, based on an analysis of the normal flow, to eliminate such feature points from the constraint intersection method, resulting in a situation where the remaining feature points generate constraint hemispheres that include the *FOE*. We can determine a lower bound on the magnitude of the normal optical flow which will eliminate all feature points whose constraint hemispheres are not guaranteed to contain the *FOE*. This results in discarding all normal flows such that

$$\|\vec{u}_{n,i}\| < v \lambda_{\max}$$

where  $v$  is an estimate of the instantaneous speed of the observer and  $\lambda_{\max}$  is the maximum allowable curvature of the path, . However this procedure will also discard feature points whose constraint hemispheres do include the *FOE*, and was not used in the experiments described below.

The case of constraint intersection for the *AOR* is very similar to that described above. The ratio  $\lambda/\rho$  should be as small as possible ( $\ll 1$ ). The minimum curvature  $\lambda_{\min}$  should be estimated and a minimum feature distance  $\rho_{\min}$  determined which bounds the  $\theta_{\omega,i}$ . If we discard all points whose normal flows satisfy

$$\|\vec{u}_{n,i}\| < \frac{v}{\rho_{\min}}$$

then the constraint hemispheres for all remaining feature points will include the *AOR*.

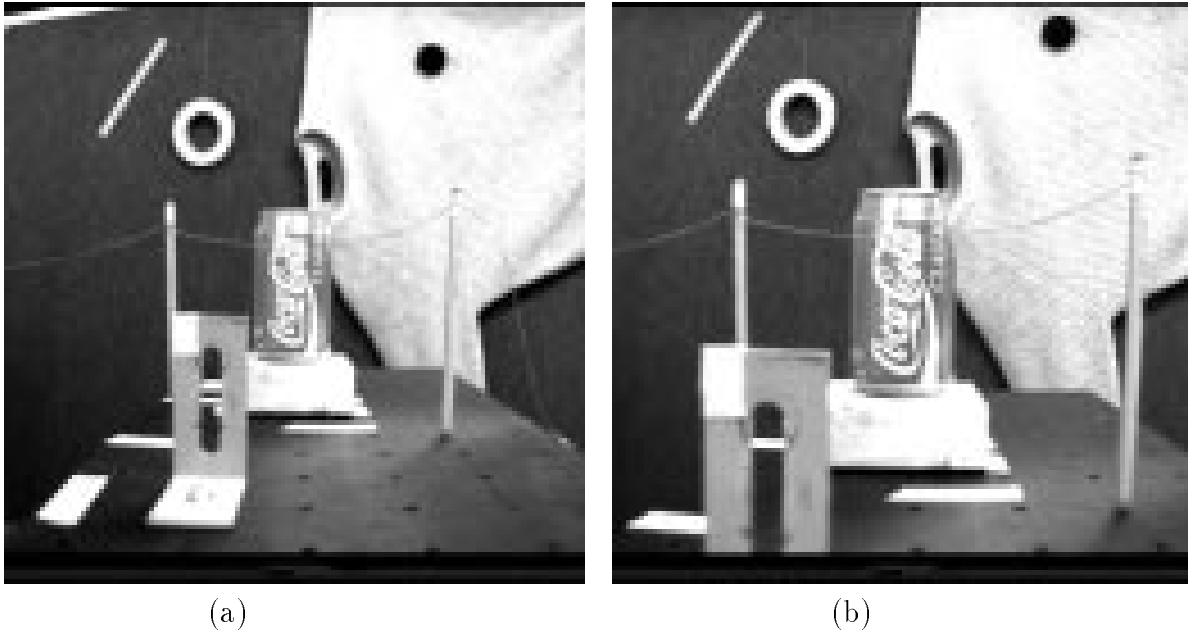


Figure 12: (a) The first frame in the sequence. (b) The last frame in the sequence.

## 8 Experiments

Two image sequences were used in our experiments. The first sequence was provided by NASA Ames Research Center; it consists of 151 frames. The motion is forward translation ( $\vec{\Omega} = \vec{0}$ ) and the *FOE* is near the centers of the images. Figure 12 displays the first and the last frames in the sequence, and Figure 13 shows the normal flow computed from frames 0, 3, and 6. Figure 14a shows the resulting accumulator array (for image points only) for the *FOE*. The solution area (defined here as the set of elements of the accumulator array which satisfy the maximum number of constraints) is very small and contains the true *FOE* (see Figure 14b).

The second image sequence was provided by the University of Massachusetts at Amherst; it consists of 30 frames. The sequence is not well calibrated and we do not have “ground truth” for it. The camera was mounted on a robot arm, and the upper arm of the robot (shoulder to elbow) was approximately parallel to the viewing direction. The lower arm (elbow to hand) was perpendicular to the upper arm. The camera was moving along a circle centered at the elbow and the viewing direction was parallel to the upper arm. Thus

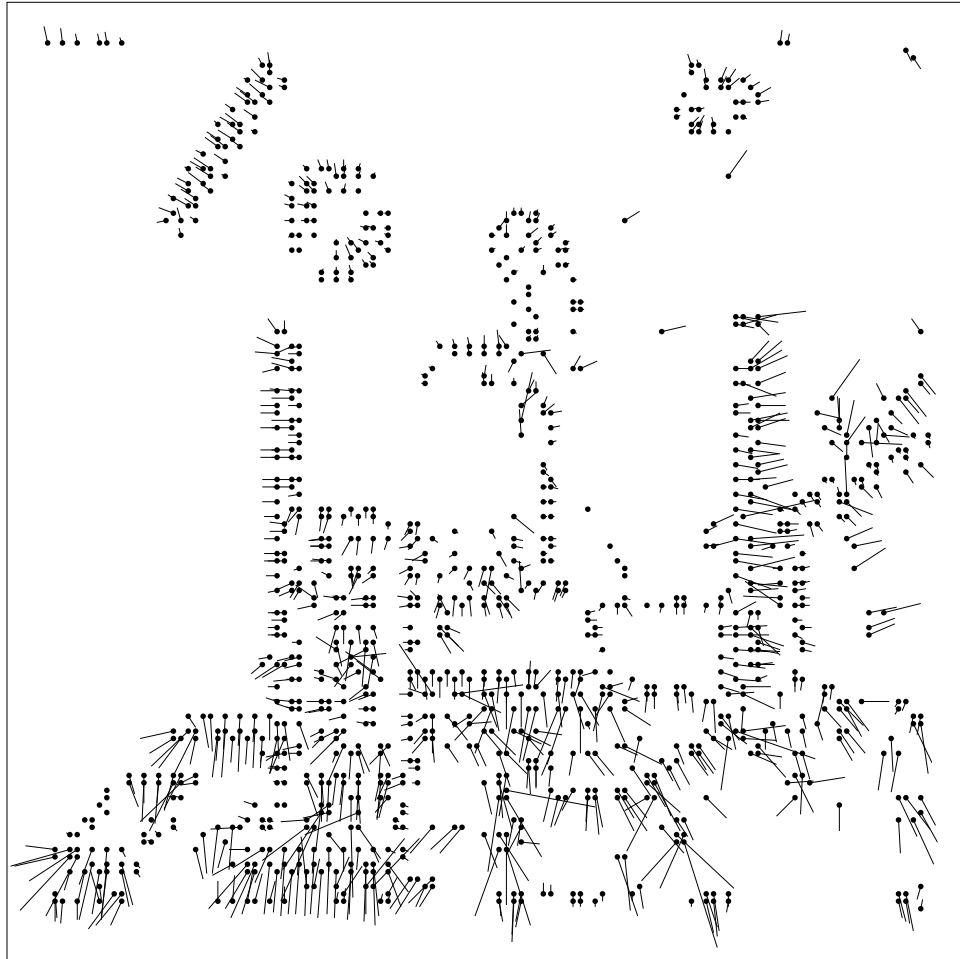
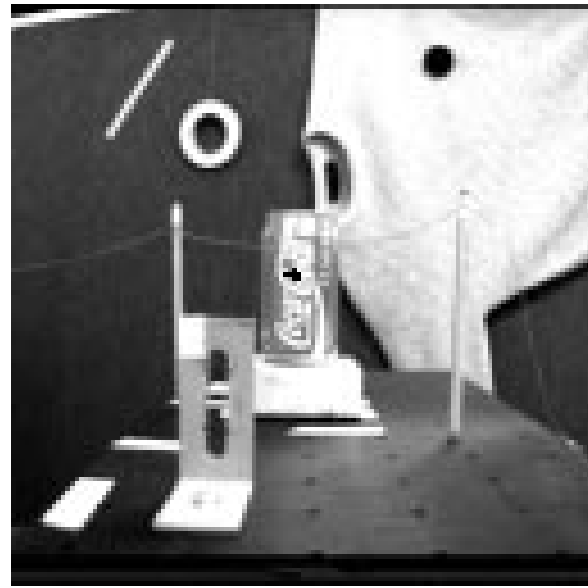


Figure 13: Normal flow computed from frames 0, 3, and 6.



(a)

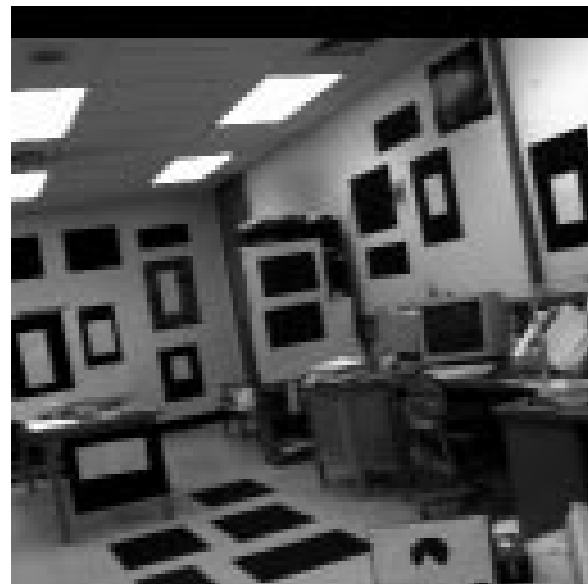


(b)

Figure 14: (a) The accumulator array for the *FOE*. The brightest points satisfy the maximum number of constraints. (b) The solution area superimposed on the third frame in the sequence (the black speck in the middle of the can).



(a)



(b)

Figure 15: (a) The first frame in the sequence. (b) The tenth frame in the sequence.

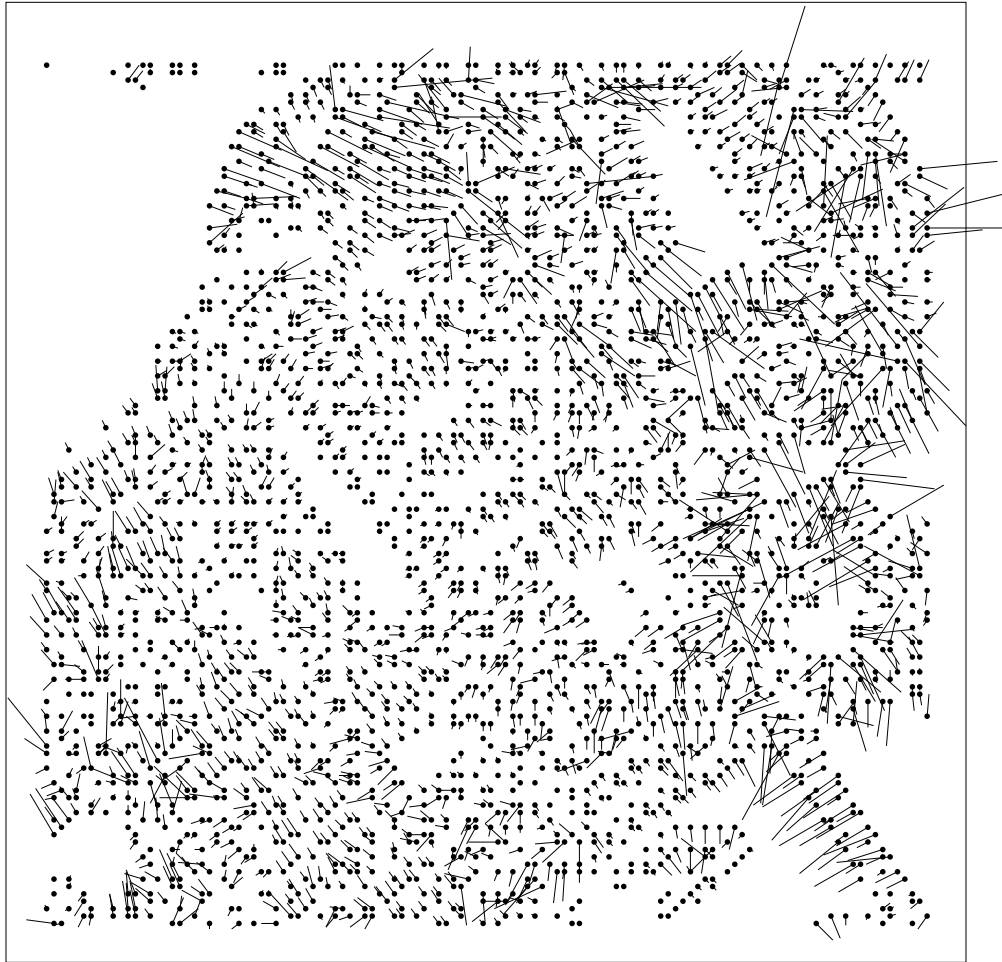


Figure 16: Normal flow computed from frames 3, 4, and 5.

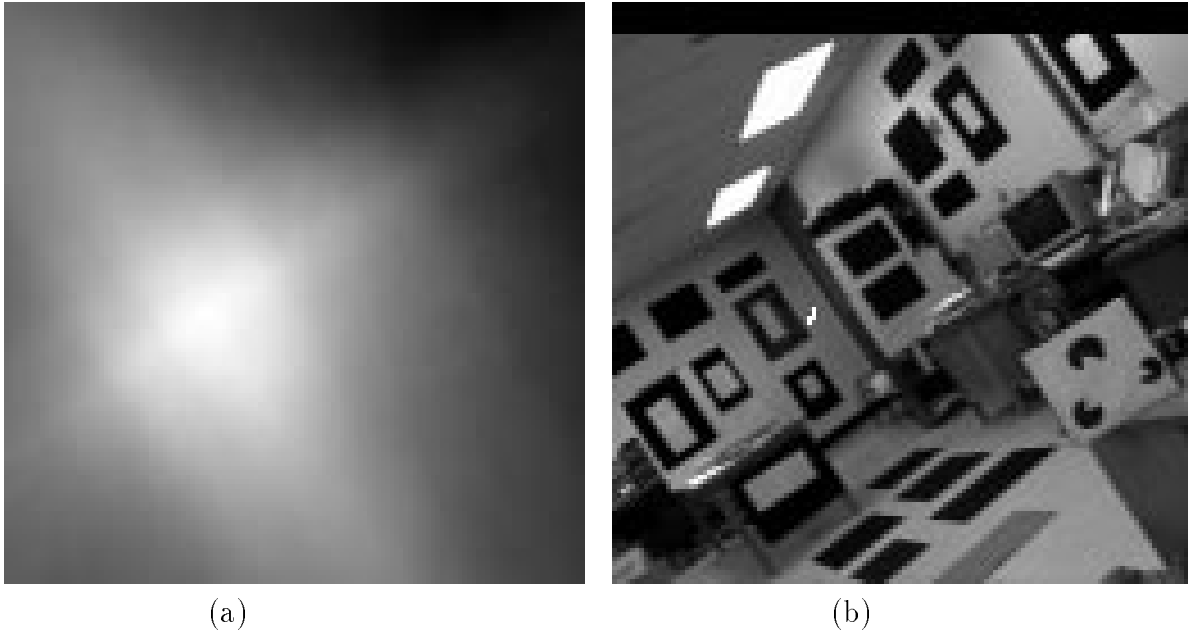


Figure 17: (a) The accumulator array for the *FOE*. The brightest points satisfy the maximum number of constraints. The solution area superimposed on the fourth frame in the sequence (the white speck close to the middle of the image).

the motion was in a plane (the torsion of the path is zero) and the viewing direction was along the binormal. The feature distance is much greater than the radius of curvature, so that rotation is dominant. Figure 15 shows the first and the tenth frames in the sequence, and Figure 16 shows the normal flow computed from frames 3, 4, and 5. Figure 17a shows the resulting accumulator array for the *AOR*. The solution area (consisting of elements of the accumulator array which satisfy the maximum number of constraints) is very small and contains the true *AOR* (see Figure 17b).

## 9 Summary

We have proposed a new model, *Frenet-Serret* motion, for the motion of an observer in a stationary environment. This model relates the motion parameters of the observer to the curvature and torsion of the path along which the observer moves. We have analyzed velocity patterns on the *IE* for different cases of the Frenet-Serret motion. We have used normal flow to derive constraints on the rotational and translational velocity of the observer

and have shown that egomotion can be computed by intersecting these constraints in the manner proposed in [6]. We have analyzed the accuracy of egomotion estimation for different combinations of observer motion and feature distance. We have suggested that feature distance should be controlled in order to make the analysis of egomotion on the basis of normal flow more reliable, and have derived the constraints on depth which make either rotation or translation dominant.

## References

- [1] J. S. Albus. Outline for a theory of intelligence. *IEEE Transactions On Systems, Man, and Cybernetics*, 21:473–509, 1991.
- [2] J. Aloimonos and C .M. Brown. The relationship between optical flow and surface orientation. In *Proc. International Conference on Pattern Recognition*, pages 542–545, 1984.
- [3] O. Bottema and B. Roth. *Theoretical Kinematics*. North–Holland, Amsterdam, 1979.
- [4] A. Bruss and B. K. P. Horn. Passive navigation. *Computer Vision, Graphics, Image Processing*, 21:3–20, 1983.
- [5] L. Dreschler and H. H. Nagel. Volumetric model and 3–d trajectory of a moving car derived from monocular tv frame sequences of a street scene. *Computer Graphics Image Processing*, 20:199–228, 1982.
- [6] Z. Durić and Y. Aloimonos. Passive navigation: an active and purposive solution. Technical Report CAR–TR–482, Computer Vision Labaratory,, Center for Automation Research, University of Maryland, College Park, 1989.
- [7] B. K. P. Horn and E. J. Weldon JR. Direct methods for recovering motion. *International Journal of Computer Vision*, 2:51–76, 1988.
- [8] B. K. P. Horn and B. G. Schunck. Determining optical flow. *Artificial Intelligence*, 17:189–203, 1981.

- [9] K. Ikeuchi. Shape from regular patterns. *Artificial Intelligence*, 22:49–75, 1984.
- [10] E. Kreyszig. *Differential Geometry*. University of Toronto Press, Toronto, Canada, 1959.
- [11] H. C. Longuet-Higgins and K. Prazdny. The interpretation of a moving retinal image. *Proceedings Royal Society London B*, 208:385–397, 1980.
- [12] S. Negahdaripour and B. K. P. Horn. A direct method for locating the focus of expansion. AI Memo 939, MIT, 1987.
- [13] D. Raviv and M. Herman. A new approach to vision and control for road following. In *Proc. IEEE Workshop on Visual Motion*, pages 217–225, 1991.
- [14] M. E. Spetsakis and J. Aloimonos. Structure from motion using line correspondences. *International Journal of Computer Vision*, 4:171–183, 1990.
- [15] C. Tomasi and T. Kanade. Factoring image sequences into shape and motion. In *Proc. IEEE Workshop on Visual Motion*, pages 21–28, 1991.
- [16] R. Y. Tsai and T. S. Huang. Uniqueness and estimation of three dimensional motion parameters of rigid objects with curved surfaces. *IEEE Transactions on Pattern Analysis and Machine Intelligence*, 6:13–27, 1984.
- [17] A. Verri and T. Poggio. Against quantitative optical flow. In *Proc. International Conference on Computer Vision*, pages 171–180, 1987.